BONE

JAK inhibition increases bone mass in steady-state conditions and ameliorates pathological bone loss by stimulating osteoblast function

Susanne Adam[1,2], Nils Simon[1,2], Ulrike Steffen[1,2], Fabian T. Andes[1,2], Carina Scholtysek[1,2], Dorothea I. H. Müller[1,2], Daniela Weidner[1,2], Darja Andreev[1,2], Arnd Kleyer[1,2], Stephan Culemann[1,2,3], Madelaine Hahn[1,2], Georg Schett[1,2], Gerhard Krönke[1,2], Silke Frey[1,2]*†, Axel J. Hueber[1,2†‡]

Janus kinase (JAK)–mediated cytokine signaling has emerged as an important therapeutic target for the treatment of inflammatory diseases such as rheumatoid arthritis (RA). Accordingly, JAK inhibitors compose a new class of drugs, among which tofacitinib and baricitinib have been approved for the treatment of RA. Periarticular bone erosions contribute considerably to the pathogenesis of RA. However, although the immunomodulatory aspect of JAK inhibition (JAKi) is well defined, the current knowledge of how JAKi influences bone homeostasis is limited. Here, we assessed the effects of the JAK inhibitors tofacitinib and baricitinib on bone phenotype (i) in mice during steady-state conditions or in mice with bone loss induced by (ii) estrogen-deficiency (ovariectomy) or (iii) inflammation (arthritis) to evaluate whether effects of JAKi on bone metabolism require noninflammatory/inflammatory challenge. In all three models, JAKi increased bone mass, consistent with reducing the ratio of receptor activator of NF-κB ligand/osteoprotegerin in serum. In vitro, effects of tofacitinib and baricitinib on osteoclast and osteoblast differentiation were analyzed. JAKi significantly increased osteoblast function ($P < 0.05$) but showed no direct effects on osteoclasts. Additionally, mRNA sequencing and ingenuity pathway analyses were performed in osteoblasts exposed to JAKi and revealed robust up-regulation of markers for osteoblast function, such as osteocalcin and Wnt signaling. The anabolic effect of JAKi was illustrated by the stabilization of β-catenin. In humans with RA, JAKi induced bone-anabolic effects as evidenced by repair of arthritic bone erosions. Results support that JAKi is a potent therapeutic tool for increasing osteoblast function and bone formation.

INTRODUCTION

In the physiologic steady-state, bone turnover is a tightly regulated process in which the rate of osteoclast-mediated resorption and osteoblast-mediated bone formation are in balance (*1*). Sex hormones and cytokines control the homeostasis of bone formation and resorption by affecting the functional state of osteoblasts and osteoclasts, respectively. Dysregulation of cytokines, which is a hallmark of chronic inflammatory diseases such as rheumatoid arthritis (RA), triggers bone loss by skewing bone homeostasis toward bone resorption and reducing bone formation (*2*, *3*).

Cytokine signaling pathways have been shown to regulate bone resorption by affecting the differentiation of osteoclasts, highlighting the role of receptor activator of nuclear factor κB (NF-κB) ligand (RANKL), macrophage colony-stimulating factor (M-CSF), and tumor necrosis factor–α (TNF-α) in the bone (*4*). However, much less is known regarding the effects of cytokine signaling pathways regulating bone formation. The Janus kinase (JAK)/signal transducers and activators of transcription (STAT) system represents a central pathway mediating the cellular response to a variety of cytokines and growth factors (*5*). A limited number of data suggest that the JAK/STAT system plays a role in bone biology as well, mainly, but not exclusively, by influencing osteoblast function. $STAT1^{-/-}$ mice exhibit increased bone density despite having increased osteoclasts (*6*), and decreased STAT1 expression has been shown to accelerate bone formation during fracture healing (*7*). The JAK/STAT pathway can be induced in osteoblasts by different inflammatory cytokines, such as oncostatin-M (OSM) or interleukin-6 (IL-6) (*8*, *9*). Considering that inflammatory cytokines have been described to dampen osteogenic induction (*10*), manipulation of JAK/STAT signaling will likely affect osteoblast differentiation or activity. Further elucidation of the role of the JAK/STAT system on bone becomes even more important when considering that highly specific JAK inhibitors, such as baricitinib and tofacitinib, have been approved for the treatment of inflammatory diseases such as RA, which are characterized by profound bone loss (*11*–*15*). Tofacitinib is a pan-JAK inhibitor with higher activity against JAK3 and JAK1 and lower activity against JAK2 (*16*–*18*). Baricitinib, on the other hand, has higher selectivity toward JAK1 and JAK2 (*17*, *18*). Both compounds exhibit marked anti-inflammatory properties and retard bone erosions in the context of inflammation (*19*, *20*). Although there have been reports about the antiresorptive capacities of JAK inhibition (JAKi), the effects of JAKi on bone are not well defined (*21*, *22*).

Here, we investigated the effect of JAKi on bone by treatment with baricitinib and tofacitinib during steady-state conditions and in mouse models of noninflammatory [ovariectomy (OVX)–induced osteoporosis] and inflammatory (serum-transfer arthritis) bone loss. We established a role of JAK inhibitors as osteoprotective agents that increase and maintain bone mass under both inflammatory and

[1]Friedrich-Alexander-University Erlangen-Nürnberg (FAU), Department of Internal Medicine 3–Rheumatology and Immunology, Universitätsklinikum Erlangen, Erlangen, Germany. [2]Deutsches Zentrum für Immuntherapie (DZI), Erlangen, Germany. [3]Nikolaus Fiebiger Center of Molecular Medicine, Universitätsklinikum Erlangen and Friedrich-Alexander University Erlangen-Nürnberg (FAU), Erlangen, Germany.
*Corresponding author. Email: silke.frey@uk-erlangen.de
†These authors jointly supervised this work.
‡Present address: Sektion Rheumatologie, Sozialstiftung Bamberg, Buger Str. 80, 96049 Bamberg, Germany.

noninflammatory conditions. This bone-protective effect of JAKi is not based on a direct effect on bone-degrading osteoclasts but rather involves an increase in the expression of osteoanabolic genes and mineralization capability of osteoblasts. JAKi led to a robust decrease in STAT3 phosphorylation, and ingenuity pathway analyses based on mRNA sequencing data revealed an increased Wnt signaling in JAK inhibitor–treated osteoblasts. These results suggest the JAK inhibitors baricitinib and tofacitinib may be useful as osteoprotective agents to reinstate bone homeostasis.

RESULTS

JAKi increases trabecular bone mass under steady-state conditions

To evaluate whether JAKi affects bone mass in vivo, 5-week-old C57BL/6 mice received the JAK inhibitor tofacitinib (50 mg/kg) or vehicle (0.5% methylcellulose and 0.025% Tween solution) once daily by oral gavage (*23*). After 6 weeks, the cohort receiving tofacitinib showed significantly increased trabecular bone mass in the tibia compared with the vehicle-treated group ($P = 0.0152$; Fig. 1, A and C), whereas trabecular bone mass in the vertebrae was not significantly affected ($P \geq 0.05$; Fig. 1, B and C). Cortical bone parameters in the tibia and the spine were not affected by JAKi (fig. S1, A and B). Serum was analyzed for the concentrations of RANKL, which promotes osteoclastogenesis, and its regulatory decoy receptor osteoprotegerin (OPG). We found that JAKi by tofacitinib significantly reduced RANKL/OPG ratio in blood serum ($P = 0.0161$; Fig. 1D). This observation suggested a systemic osteoanabolic effect of JAKi, potentially providing an explanation for the increased bone mass. Moreover, regulation of the RANKL/OPG ratio indicated the potential involvement of osteoblasts and osteocytes, which represent the major source of both RANKL and OPG under steady-state conditions. Histomorphometric analysis of tibial bone sections did not show any change in osteoblast nor osteoclast numbers (fig. S1, C and D).

JAKi mitigates OVX-induced bone loss

To clarify whether JAKi maintains its osteoanabolic function in pathological bone loss, we investigated the effect of JAKi on OVX-induced osteopenia in a therapeutic setting. C57BL/6 mice were ovariectomized at 8 weeks of age, and bone loss was allowed to establish for 14 days, after which mice received the JAK inhibitor tofacitinib (50 mg/kg), the JAK inhibitor baricitinib (10 mg/kg), or vehicle twice daily for 6 weeks. Weight development over time and uterus degeneration compared with the sham-treated group confirmed that OVX had been established (fig. S2, A to H), in line with bone loss (Fig. 2, A to C). Both JAK inhibitors increased trabecular thickness; treatment with baricitinib resulted in significantly elevated trabecular bone mass in both tibia and vertebra ($P < 0.05$; Fig. 2, A to C). Cortical bone was not affected (fig. S2, I to K). With respect to RANKL and OPG concentrations, RANKL was increased after OVX in vehicle-treated mice, which is reflected by elevated RANKL/OPG ratio (Fig. 2D). In contrast, when ovariectomized mice had received JAK inhibitors, RANKL concentration returned to baseline and RANKL/OPG ratio was reduced compared with the OVX vehicle–treated group (Fig. 2D). Histomorphometric analysis of tibiae did not show any change in the numbers of tartrate-resistant acid phosphatase–positive ($TRAP^+$) multinucleated osteoclasts (fig. S2L) or osteoblasts after JAK inhibitor treatment (fig. S2M).

JAKi halts bone loss in the context of arthritis

To assess the effects of JAKi on bone homeostasis during inflammatory bone loss, we analyzed JAKi using the K/BxN serum-transfer mouse model of arthritis (STA). For this purpose, C57BL/6 mice were injected with K/BxN serum (150 μl) intraperitoneally at 8 weeks of age, after which they received tofacitinib (50 mg/kg), baricitinib (10 mg/kg), or vehicle treatment twice daily for 14 days. Clinical parameters showed that mice during JAKi maintained their weight and grip strength and developed little ankle or paw swelling, in accordance with diminished arthritis scores (Fig. 3, A to C, fig. S3, A and B). Micro–computed tomography (μCT) analysis of tibia revealed that trabecular bone density was increased in STA mice receiving JAK inhibitors compared with vehicle-treated STA mice, an effect that was primarily a consequence of increased trabecular thickness (Fig. 3, D and F). In contrast to noninflammatory conditions, cortical bone was also protected by JAKi, as shown by increased cortical thickness and, in the case of baricitinib, higher cortical area fraction compared with mice treated with vehicle (Fig. 3E). Histomorphometry of tibial bone again showed no difference in osteoblast numbers, whereas osteoclasts were increased with respect to arthritis induction and returned to baseline upon JAK inhibitor treatment (fig. S3, C and D).

JAKi does not affect osteoclastogenesis or osteoclast function

To elucidate the mechanism of the bone-protective effect of JAKi, we first investigated whether JAKi affects bone-resorbing osteoclasts. Therefore, mononuclear cells were isolated from the bone marrow of mice and from the peripheral blood of humans to assess the effect of tofacitinib or baricitinib on RANKL-induced osteoclastogenesis, using JAK inhibitor concentrations that are well established (*24*–*27*). In the human system, both JAK inhibitors did not impair the differentiation of multinucleated $TRAP^+$ osteoclasts (Fig. 4, A and B). Similar results were found in the murine system: Neither tofacitinib nor baricitinib reduced the differentiation of multinucleated $TRAP^+$ osteoclasts (Fig. 4, C to F). Although the number of osteoclasts was unaffected, the capability of osteoclasts to resorb bone might be altered by JAKi. However, neither JAK inhibitor impaired the bone-resorbing capacity of osteoclasts, as shown by bone resorption assays performed on bone matrix–coated surfaces (Fig. 4, G and H).

JAKi increases osteoblast function and mineralization activity and alters osteoblast gene networks

Having observed no effect of JAKi on osteoclasts, we suspected that JAKi may instead affect bone-forming osteoblasts. We induced mesenchymal stem cells (MSCs) using osteogenic cell culture medium to undergo osteoblastogenesis and synthesize extracellular calcium deposits. When treated with tofacitinib or baricitinib, mineralization capability significantly increased as tested by Alizarin Red staining ($P < 0.05$; Fig. 5A). Similar results were found when testing the mineralization potential of primary calvaria-derived osteoblasts, which was increased upon stimulation with the JAK inhibitor tofacitinib (Fig. 5B). On the basis of the cell culture results that suggested no effect of JAKi on osteoclasts but stimulation of osteoblasts, we performed an in-depth analysis of the effects of JAKi on the genomic transcriptional network of osteoblast gene expression. Whole transcriptome RNA sequencing (RNAseq) was performed on MSC-derived osteoblasts 1 day after osteogenic induction (Fig. 5C). Treatment with baricitinib altered approximately 1300 genes with a

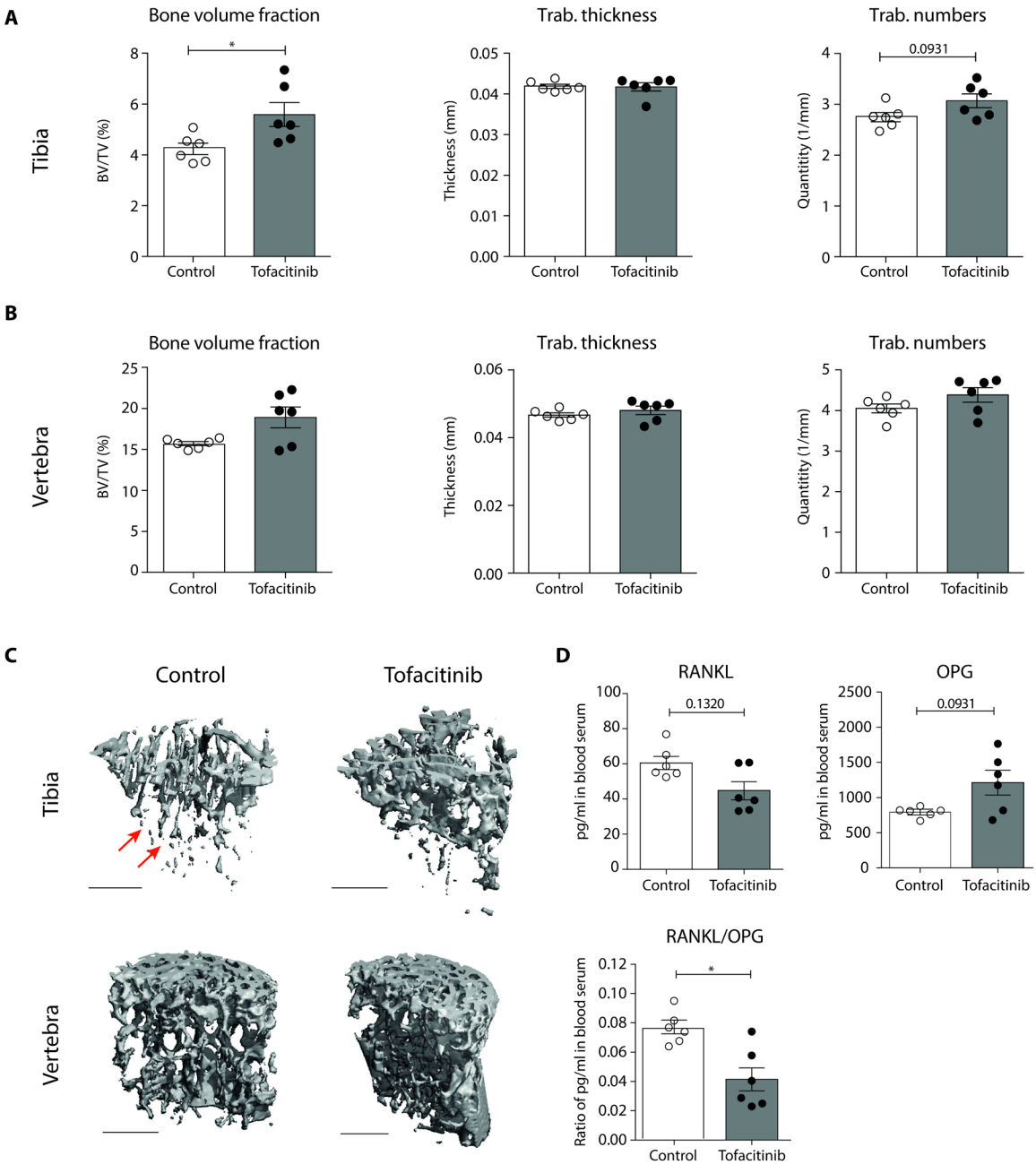

Fig. 1. JAKi increases trabecular bone mass under steady-state conditions. C57BL/6 mice (5 weeks old) received tofacitinib (50 mg/kg) or 0.5% methylcellulose and 0.025% Tween solution as vehicle (control) once daily by oral gavage for 6 weeks. Trabecular (trab) bone phenotype was quantified by μCT, and serum was analyzed by ELISA. (**A** and **B**) μCT quantification of trabecular bone mass in tibiae and vertebrae. Trabecular bone volume/total volume (BV/TV), trabecular thickness, and trabecular numbers are shown. (**C**) Representative μCT images of trabecular bone in tibiae (top) and vertebrae (bottom). Arrows indicate regions of decreased trabecular density. Scale bars, 500 μm. (**D**) RANKL and OPG serum concentrations and RANKL/OPG ratio. Data are presented as means ± SEM. Statistical significance was calculated by Mann-Whitney *U* test (*$P < 0.05$, $n = 6$).

false discovery rate (FDR) of 0.1 compared with vehicle, and tofacitinib affected approximately 1800 genetic targets at the same FDR. By that, between 190 and 239 analysis-ready molecules were obtained for tofacitinib- and baricitinib-treated MSCs, respectively, compared with vehicle-treated cells. Changes in gene expression for both JAK inhibitors varied in a range between 0.2- and 2.2-fold. Of these effects, few genes were compound specific, whereas the vast majority of genes were affected by both JAK inhibitors. As expected, and validating the accuracy of mRNA sequencing data, canonical pathway analysis of gene expression revealed IL-6 and OSM signaling as the prominent pathways, which were targeted upon JAKi (fig. S4A). In accordance, expression of glycoprotein 130 (*Gp130*; 0.90-fold), OSM-specific receptor subunit (*Osmr*; 0.41-fold), *Jak3* (0.71-fold), *Stat3* (0.68-fold), and suppressor of cytokine signaling 3 (*Socs3*;

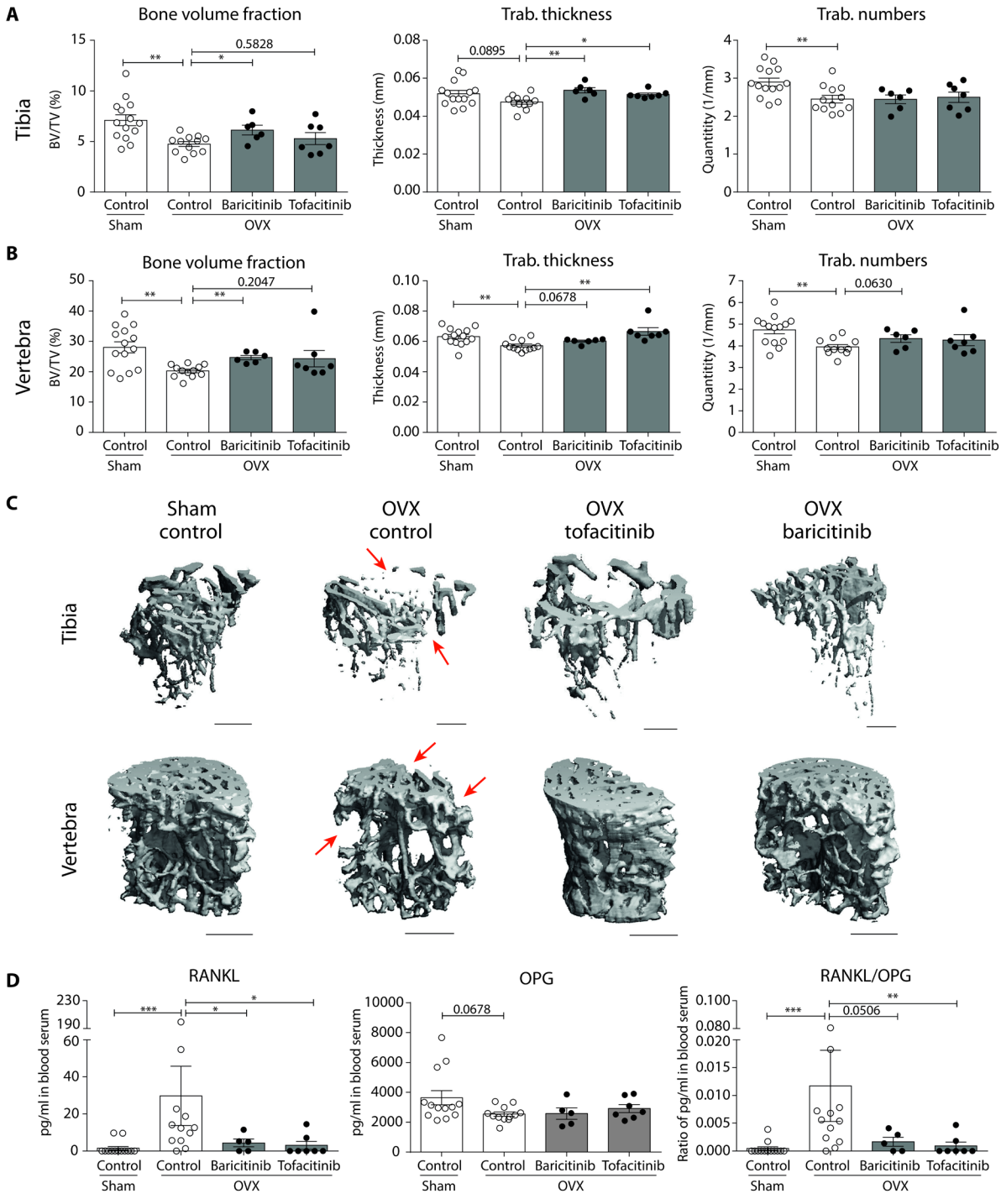

Fig. 2. JAKi mitigates OVX-induced bone loss. C57BL/6 (8 weeks old) mice were bilaterally ovariectomized or underwent sham surgery. Bone loss was allowed to establish for 2 weeks. Mice then started to receive tofacitinib (50 mg/kg), baricitinib (10 mg/kg), or vehicle (control) twice daily by oral gavage for 6 weeks. Trabecular (trab) bone phenotype was quantified by μCT, and serum was analyzed via ELISA. (**A** and **B**) μCT quantification of trabecular bone mass in tibiae and vertebrae. Trabecular bone volume/total volume, trabecular thickness, and trabecular numbers are shown. (**C**) Representative μCT images of trabecular bone in the tibiae (top, each) and vertebrae (bottom, each) of mice receiving vehicle, tofacitinib, or baricitinib. Arrows indicate regions of decreased trabecular density. Scale bars, 500 μm. (**D**) RANKL and OPG serum concentrations and RANKL/OPG ratio. Data are presented as means ± SEM. Statistical significance was calculated by Mann-Whitney *U* test (*$P < 0.05$, **$P \leq 0.01$, and ***$P \leq 0.001$, $n = 5$ to 14).

0.59-fold) were significantly down-regulated ($P < 0.05$; fig. S4A). Furthermore, analysis of STAT phosphorylation in MSCs, which were induced to undergo osteoblastogenesis, showed that JAKi using either agent effectively blocked inducible STAT3 phosphorylation, whereas STAT1 was not phosphorylated in osteoblasts (Fig. 5, D and E). Ingenuity pathway analysis for upstream regulators showed

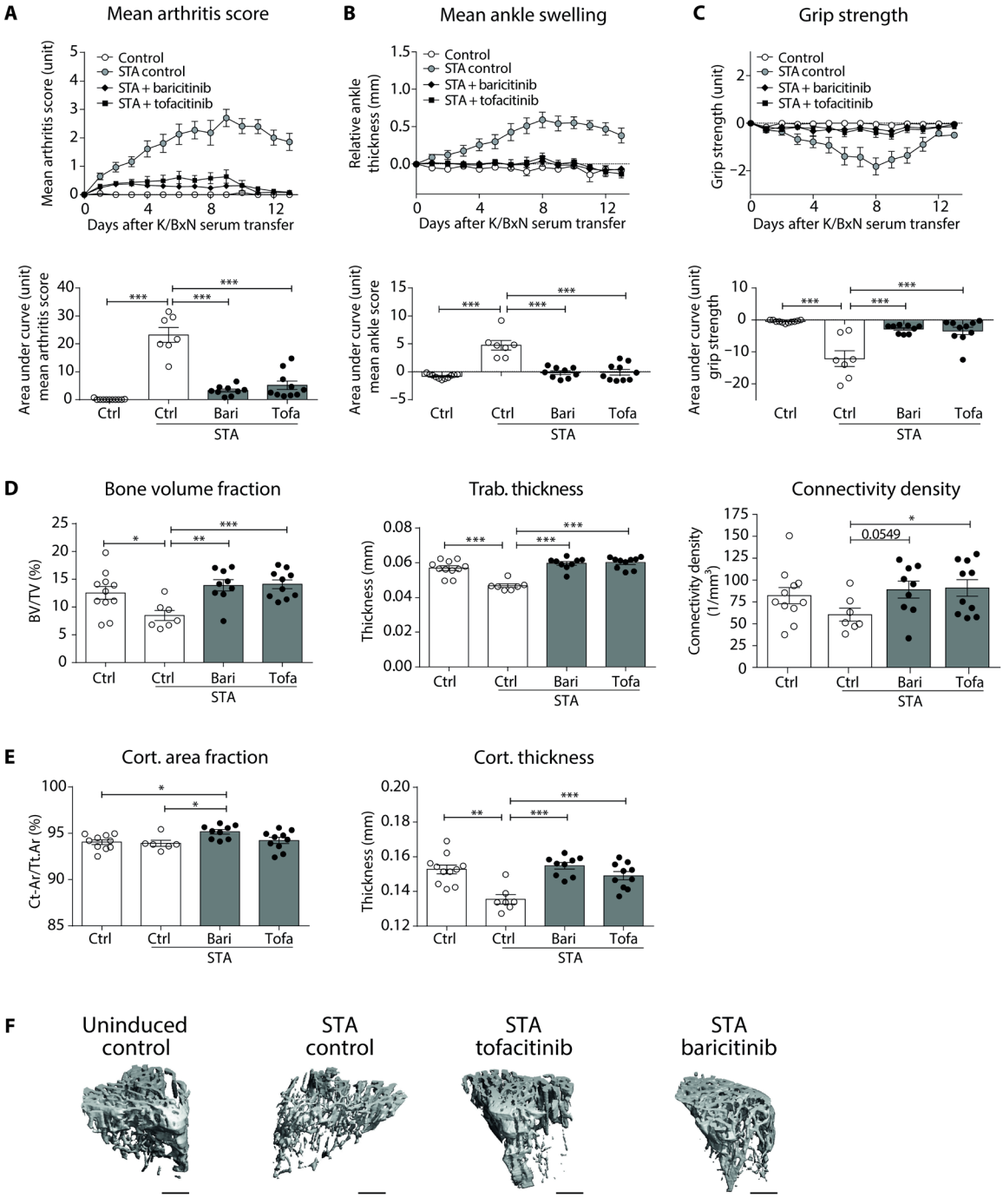

Fig. 3. JAKi halts bone loss in the context of arthritis. C57BL/6 mice (8 weeks old) induced for serum-transfer arthritis (STA) received treatment with tofacitinib (50 mg/kg), baricitinib (10 mg/kg), or vehicle [control (ctrl)] twice daily by oral gavage for 2 weeks. An uninduced group, receiving vehicle twice daily by oral gavage, accompanied the experiment. Animals were scored daily for clinical disease parameters. Trabecular (trab) and cortical (cort) bone phenotype was quantified by μCT. (**A** to **C**) Clinical arthritis score, ankle swelling, and grip strength (top) and quantification of area under the curve (bottom). (**D** and **E**) μCT quantification of trabecular and cortical bone phenotype in tibiae. (D) Trabecular bone volume/total volume (BV/TV), trabecular thickness, and connectivity density. (E) Cortical bone area/total cross-sectional area inside the periosteal envelope (Ct.Ar/Tt.Ar) and cortical thickness. (**F**) Representative μCT images of tibial trabecular bone in uninduced mice and STA mice receiving vehicle, tofacitinib, or baricitinib. Scale bars, 500 μm. Data are expressed as means ± SEM. Statistical significance was calculated by one-way ANOVA with Dunnett post hoc test (*$P < 0.05$, **$P \leq 0.01$, and ***$P \leq 0.001$, $n = 7$ to 11).

the expected down-regulation of upstream inflammatory mediators upon JAKi of osteoblasts, in particular those directly related to JAK/STAT signaling, but also others such as *Tnf-α* and *Il-17*, which have been reported to dampen osteoblast activity (Fig. 5F). In contrast, when applying the ingenuity pathway analysis to upstream regulators that are induced by JAKi in osteoblasts, a Wingless/Int-1 (Wnt)

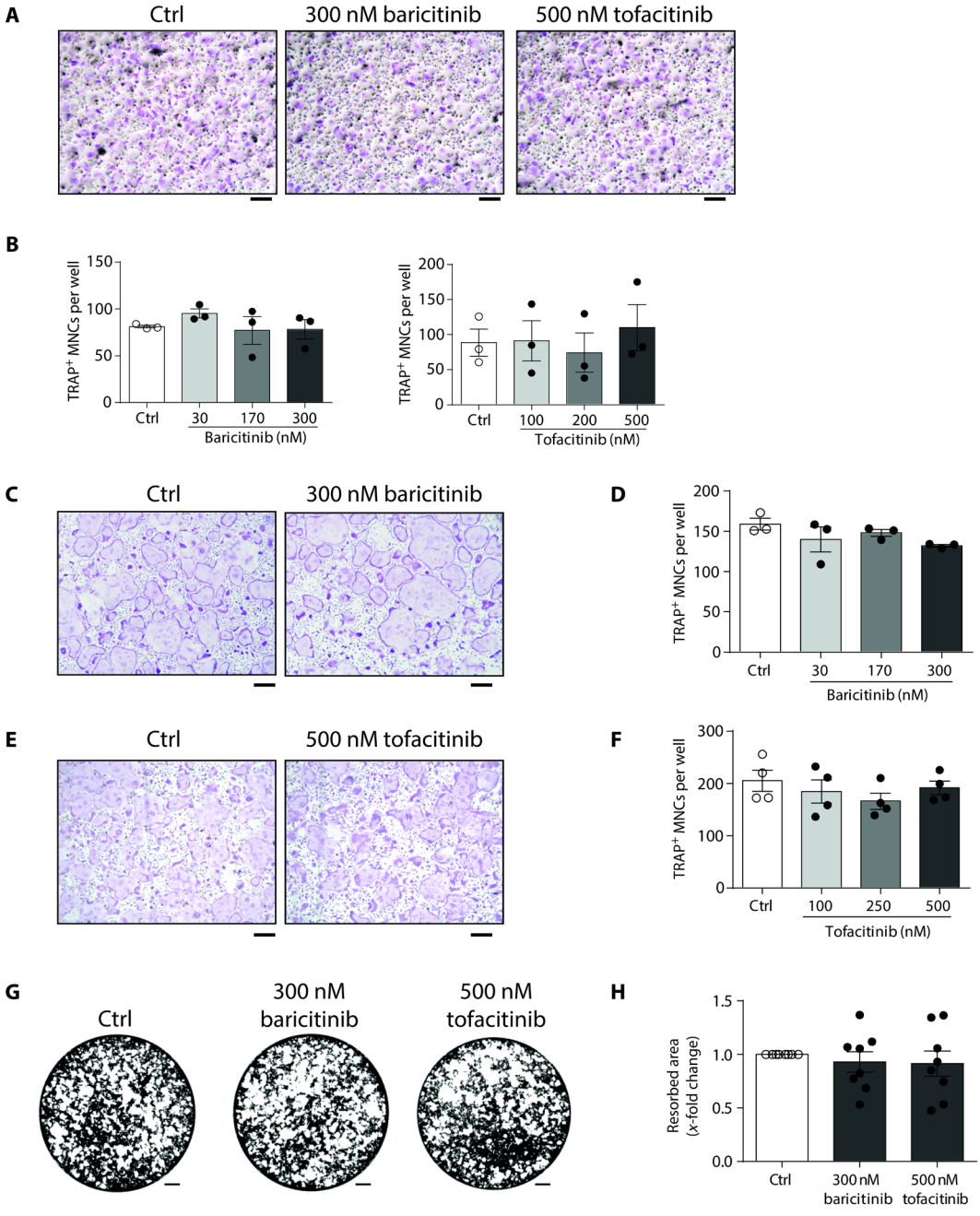

Fig. 4. JAKi does not affect osteoclastogenesis or osteoclastic bone resorption. Osteoclasts were differentiated from human peripheral blood mononuclear cells or murine bone marrow cells in the presence or absence of JAK inhibitors. Osteoclasts were stained for TRAP and quantified. Osteoclastic resorption capability was evaluated by culturing osteoclasts in calcium phosphate matrix–coated wells and by quantifying the remaining calcium phosphate matrix. (**A** and **B**) Human osteoclastogenesis assays showing (A) representative microphotographs and (B) quantification of osteoclast numbers in untreated (control), baricitinib-, or tofacitinib-treated conditions. $TRAP^+$ cells appear purple. Scale bars, 500 μm ($n = 3$). (**C** to **F**) Murine osteoclastogenesis assays showing (C and E) representative microphotographs of (C) baricitinib- and (E) tofacitinib-treated samples, respectively, compared with the untreated control. $TRAP^+$ cells appear purple. Scale bars, 500 μm. (D and F) Quantification of murine osteoclast numbers of (D) baricitinib- and (F) tofacitinib-treated conditions, respectively, compared with untreated control sample ($n = 3$ to 4). (**G** and **H**) Von Kossa staining of calcium phosphate matrix–coated wells after murine osteoclastogenesis. The black area is the remaining calcium phosphate matrix, and the white area indicates resorbed spots. (G) Representative images of untreated (control), baricitinib-, and tofacitinib-treated conditions. (H) Quantification of von Kossa staining ($n = 8$). Scale bars, 500 μm. Data are expressed as means ± SEM. Statistical significance was calculated by one-way ANOVA with Dunnett post hoc test.

signature was observed with up-regulation of Wnt1, Wnt3A, and Wnt5A pathways (Fig. 5F). In-depth network analysis was conducted subsequently (fig. S4B), showing that osteocalcin (*Ocn*, *Bglap2*; 1.38-fold) expression emerged as a central target downstream of various osteoanabolic genes. In addition, network analysis revealed osterix (*Osx*, *Sp7*; 1.19-fold), transmembrane protein 119 (*Tmem119*;

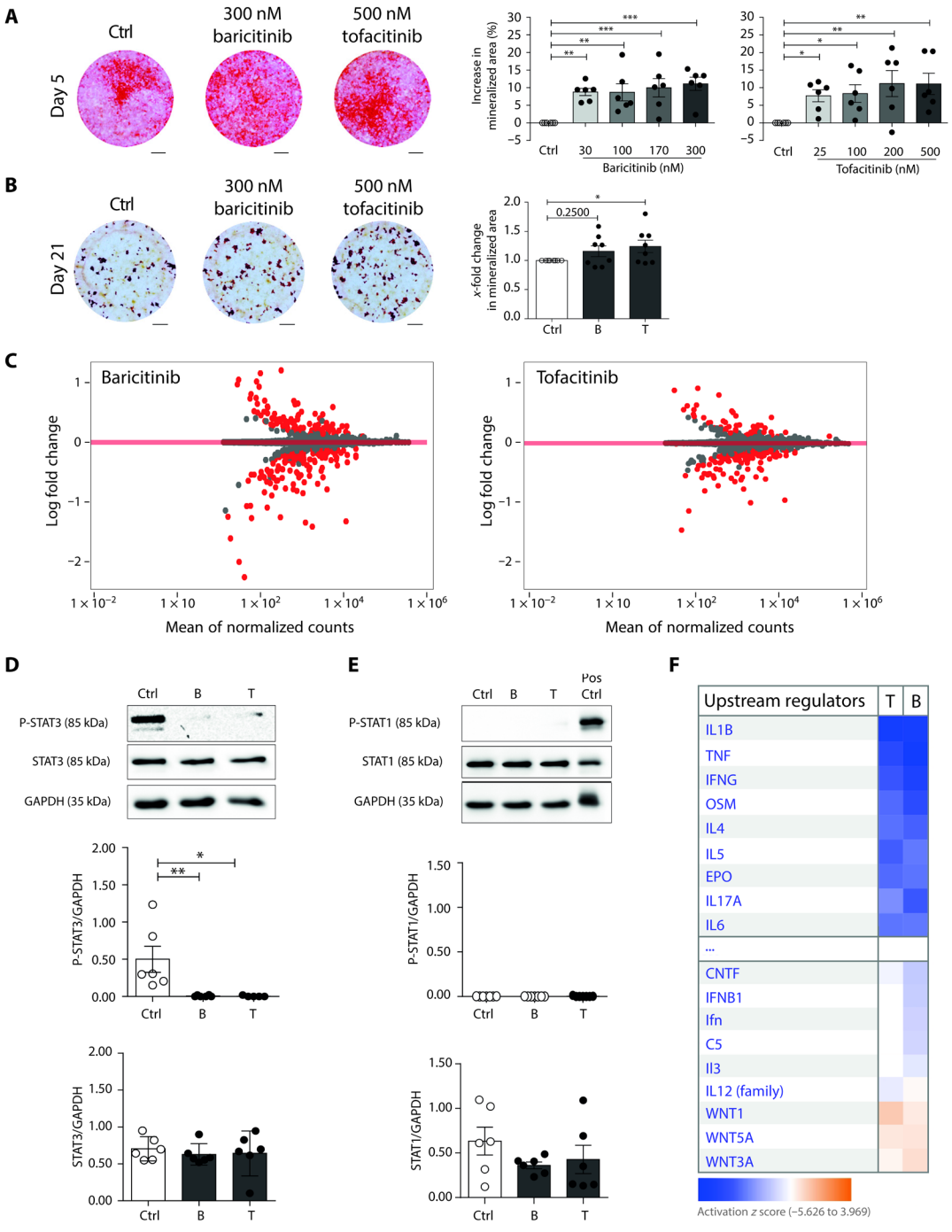

Fig. 5. JAKi induces an anabolic network in osteoblasts supporting osteoblastogenesis. Osteoblastogenesis was induced in MSC- and calvaria-derived osteoblasts challenged with dimethyl sulfoxide (DMSO) vehicle control, 300 nM baricitinib (B), 500 nM tofacitinib (T), or as indicated. (**A**) Representative photographs and quantification of calcium nodules deposited by MSC-derived osteoblasts and stained with Alizarin Red after 5 to 6 days of osteogenic induction. Scale bars, 5 mm ($n = 6$). (**B**) Representative photographs and quantification of calcium nodules deposited by calvaria-derived osteoblasts and stained with Alizarin Red after 21 days of osteogenic induction. Scale bars, 5 mm ($n = 8$). (**C**) RNAseq analysis of MSC-derived osteoblasts 1 day after osteogenic induction. Minus-Average (MA) plots for baricitinib- and tofacitinib-treated MSCs compared with vehicle control. Red and gray dots show genes with adjusted P value below or above 0.1, respectively ($n = 4$). (**D** and **E**) During osteoblastogenesis of MSCs, intracellular protein content was analyzed by Western blot ($n = 5$ to 6). (D) Representative Western blot for P-STAT3 and STAT3, with glyceraldehyde-3-phosphate dehydrogenase (GAPDH) as loading control (top) and quantification of P-STAT3 and STAT3 (bottom panels). (E) Representative Western blot for P-STAT1 and STAT1, P-STAT1–positive control (Pos Ctrl), with GAPDH as loading control (top) and quantification of P-STAT1 and STAT1 (bottom panels). (**F**) Ingenuity pathway analysis for upstream mediators: Shades of blue and orange indicate decreased and increased activation z score, respectively. Data are expressed as means ± SEM. Statistical significance was calculated by (A and B) repeated-measures ANOVA and (D and E) one-way ANOVA with Dunnett post hoc test (*$P < 0.05$, **$P \leq 0.01$, and ***$P \leq 0.001$).

1.32-fold), TSC22 domain family protein 3 (*Tsc22d3*; 1.15-fold), and insulin-like growth factor-binding protein 5 (*Igfbp5*; 1.09-fold) were part of the network of genes induced by JAKi in osteoblasts (fig. S4B). In contrast, catabolic genes, such as matrix metalloproteinase 13 (*Mmp13*; 0.44-fold), were down-regulated by JAKi (fig. S4B).

JAKi induces osteocalcin expression in osteoblasts

In accordance with the RNAseq data, quantitative polymerase chain reaction (qPCR) showed that *Ocn* expression was increased by JAK inhibitor treatment as early as 1 day after osteogenic induction (Fig. 6A). In contrast, *Runx2* expression was not affected by JAKi (Fig. 6B), and markers of adipocyte differentiation, such as fatty acid binding protein 4 (*Fabp4*), were down-regulated by JAKi (Fig. 6C). Further confirming these findings, when primary calvaria-derived osteoblasts were analyzed, JAKi induced increased expression of *Ocn* (Fig. 6D) and decreased expression of *Rankl* (Fig. 6E). In line with the observation of an induced Wnt signaling and the increased expression of osteocalcin in osteoblasts challenged with JAK inhibitors, the expression of Wnt1 and the key component of Wnt signaling, β-catenin, was induced after exposing osteoblasts to

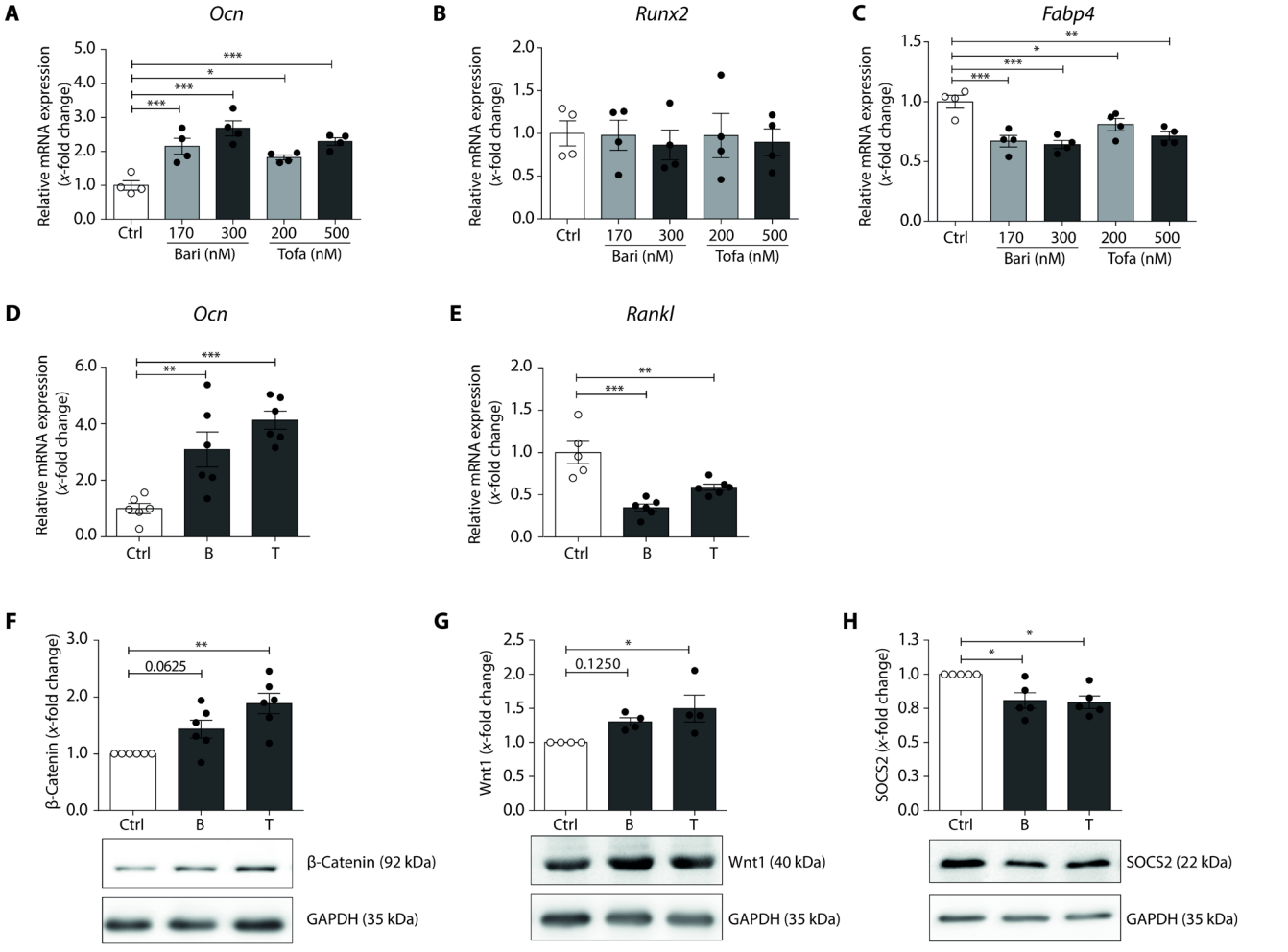

Fig. 6. JAKi increases Wnt1 and β-catenin protein expression in osteoblasts and induces repair of bone erosions. Osteoblastogenesis was induced in MSC- and calvaria-derived osteoblasts, with DMSO vehicle control, 300 nM baricitinib (B), 500 nM tofacitinib (T), or as indicated. (**A** to **C**) qPCR analysis of gene expression at day 1 in MSC-derived osteoblasts ($n = 4$). (**D** and **E**) qPCR analysis of gene expression at day 21 in calvaria-derived osteoblasts ($n = 6$). (**F** to **H**) During osteoblastogenesis of MSCs, intracellular protein content was analyzed by Western blot. Representative Western blots for (F) β-catenin, (G) Wnt1, and (H) SOCS2 with GAPDH as loading control and corresponding quantification of protein quantity ($n = 4$ to 6). Data are expressed as means ± SEM. Statistical significance was calculated by (A to E) one-way ANOVA and (F to H) repeated-measures ANOVA, each with Dunnett post hoc test (*$P < 0.05$, **$P \leq 0.01$, and ***$P \leq 0.001$).

JAK inhibitors (Fig. 6, F and G), whereas Wnt3A and Wnt5A were not regulated by JAKi (fig. S4, C and D). In addition, suppressor of cytokine signaling 2 (SOCS2), which has been described to bind β-catenin (*28*) and act as a negative regulator of β-catenin (*29*), was significantly down-regulated by both JAK inhibitors ($P < 0.05$; Fig. 6H). SOCS3, on the other hand, showed no significant alteration with respect to either baricitinib or tofacitinib ($P > 0.05$; fig. S4E).

JAKi induces repair of bone erosions in humans

To translate these effects to humans, we searched for evidence of increased osteoblast activity and bone repair in patients treated with JAK inhibitors. Tofacitinib and baricitinib are approved for the treatment of RA (*11*–*14*) and have been shown to inhibit the progression of inflammatory bone erosion in the disease. However, evidence for bone repair in patients treated with either one of these two agents has not yet been reported. We explored this concept in two patients who received the JAK inhibitor tofacitinib (5 mg, twice daily) for treatment of RA. Patients received longitudinal high-resolution CT scans of their metacarpophalangeal joints, which allowed for a detailed depiction of the bone architecture, particularly the accurate visualization of bone repair. Follow-up scans showed evidence of substantial reduction in erosion size, supporting the concept that JAKi exerts bone-anabolic functions leading to erosion repair (Fig. 7).

DISCUSSION

Growing evidence recognizes the importance of JAK/STAT signaling in the pathophysiology of inflammatory diseases such as RA and colitis. Apart from that, JAK/STAT signaling may also affect bone homeostasis (*30*). JAK inhibitors have already entered clinical use for the treatment of RA (*11*–*14*), and their application for a variety of other diseases is currently being developed. How JAK/STAT inhibition affects bone homeostasis, however, is not fully understood. Many cytokines, some of which have supposed bone-degrading properties and bone-protective properties, signal through the JAK/STAT system. Individual cytokines that signal through JAK/STAT

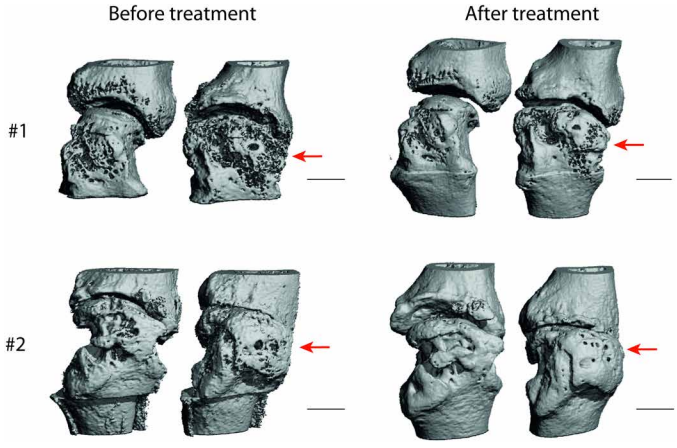

Fig. 7. JAKi by tofacitinib induces repair of bone erosions in patients with RA. 3D HR-pQCT images of metacarpophalangeal joints were generated before (left, each) and after treatment (right, each) from patients with RA ($n = 2$) who received 5 mg of tofacitinib twice daily for (top) 4 years and (bottom) 2 years. Scale bars, 5 mm. Arrows indicate exemplary regions of erosion where bone formation occurred.

may have heterogeneous effects on bone (*9*, *31*–*33*). To analyze the implications of JAKi for bone metabolism, we made use of two JAK inhibitors, tofacitinib and baricitinib, which are currently used for the treatment of RA. They differ in their inhibitory specificities against JAK family members. Whereas baricitinib preferentially inhibits JAK1 and JAK2, tofacitinib is reported to have a high degree of selectivity against JAK3, JAK1, and, to a lesser extent, JAK2 (*16*–*18*).

Herein, we demonstrate that JAKi has beneficial effects on bone in various models. Unexpectedly, even in steady-state conditions, treatment with JAK inhibitors led to a modest but consistent increase in trabecular bone mass in mice, suggesting that the effect of JAK inhibitors such as tofacitinib and baricitinib is not exclusively based on their anti-inflammatory function but instead due to direct effects on bone. In accordance, JAKi also mitigated OVX-induced osteoporosis, which is not "inflammatory" in nature per se. The effects of JAKi on OVX-induced osteoporosis were more pronounced than on bone under steady-state conditions, suggesting that the effects of JAKi on T cell activation, which is part of the pathophysiology of OVX-induced osteoporosis, may additionally contribute to the bone-protective effects of JAKi in this model (*34*). In the arthritis model, JAKi protected from local inflammatory and systemic bone loss. Although the effect on local bone erosions and joint protection is likely due to the antiarthritic effect of JAKi, which has been reported previously (*21*, *22*, *26*, *35*), the effect on systemic bone is interesting and additionally points to a direct bone-sparing effect of JAKi. Hence, a consistent bone-protective function of JAKi was observed across a variety of models.

Data using murine and human osteoclasts showed that JAKi exhibits no direct effect on the differentiation and function of bone-degrading osteoclasts. Consequently, other mechanisms appear to contribute to the bone-sparing effects of JAKi. Previous studies have also shown that JAKi may not directly affect osteoclastogenesis (*22*) but instead indirectly blunt bone resorption through altering RANKL production in mesenchymal cells. This signature was observed in our models treated with JAK inhibitors, which showed lower *Rankl* expression, indicating drug effects on the osteoblast lineage. Furthermore, impaired differentiation of osteoblasts and lower bone formation are part of the pathophysiology of bone loss in the context of arthritis (*36*), and down-regulation of Wnt-induced bone formation has been suggested to play a key role in arthritic bone loss (*37*). On the basis of these observations, we hypothesized that JAKi may modulate osteoblast function and potentially affect key osteoblast signaling pathways such as Wnt.

Ingenuity pathway analysis of mRNA sequencing data revealed a limited number of upstream regulators that were enhanced upon JAKi, all of which were Wnt proteins (Wnt1, Wnt5A, and Wnt3A), central promoters for bone formation (*38*, *39*). Cross-talk between STAT3 and the Wnt pathway has been previously reported, particularly related to cell survival and proliferation (*40*, *41*). STAT3 has been shown to suppress Wnt signaling and promote its degradation (*42*–*44*). A proposed model includes direct interaction between STAT3-induced SOCS and β-catenin, by which β-catenin degradation is enhanced (*29*, *42*). Therefore, down-regulation of STAT3, and consequently SOCS, can promote stabilization of β-catenin, culminating in the up-regulation of osteoanabolic factors, such as osteocalcin (*45*). We verified this by exposing osteoblasts to JAK inhibitors, noting reduced activated STAT3 in osteoblasts, which was accompanied by increased Wnt1, stabilization of β-catenin, decreased SOCS2 expression, increased expression of osteoanabolic genes such as osteocalcin, and higher mineralization capacity of osteoblasts. In addition, the decreased RANKL production, which has been a consistent signal in JAK inhibitor–treated mice, can be attributed to reduced STAT3 signaling (*46*), as modeled in fig. S5.

These findings may have substantial consequences for the treatment of bone loss associated with arthritis, for which JAK inhibitors are already used. Current concepts suggest that the bone protective effect of antirheumatic drugs is related to the inhibition of osteoclast differentiation, which to some extent holds true for cytokine inhibitors targeting TNF-α and IL-1 (*4*). On the other hand, clinical data on IL-6R inhibition, which targets the JAK/STAT pathway, have shown that inhibition of IL-6R increases osteocalcin, indicative of enhanced bone formation (*47*). This would imply that existing bone damage could be repaired if an osteoanabolic environment could be restored and that JAKi would be a clinical strategy to accomplish this. Using a technique that allows visualization of bone in humans at high resolution, we found preliminary evidence that JAKi allowed repair of existing bone erosions in patients with RA, validating the concept in humans. These data provide the rationale for looking at bone repair upon JAK inhibitor treatment in a prospective setting in larger groups of patients.

Some limitations of this study should be acknowledged. The effect of baricitinib could not be fully analyzed in steady-state conditions. Moreover, the transfer of our in vitro findings to the in vivo situation is challenged by the ubiquity of JAK signaling and the plethora of cell types affected by JAKi, whereas our in-depth focus remained on the key regulators in bone homeostasis, osteoblasts and osteoclasts. Furthermore, the ramifications of this study for potential clinical applications need further investigation. Other limitations include the relatively small sample sizes, especially with respect to the human high-resolution quantitative CT (HR-pQCT) data, which did not allow for statistical analysis.

Together, this study shows that JAKi directly supports the function of bone-forming osteoblasts by enhancing the Wnt signaling pathway. This effect leads to an increase in bone mass under steady-state conditions, consistent mitigation of pathological bone loss, and repair of bone erosions in arthritis. Hence, JAK inhibitors

should be considered bone-active drugs, in addition to their established role as immune regulatory interventions.

MATERIALS AND METHODS

Study design

The objective of this study was to investigate the effect of JAKi on bone metabolism using two clinically approved JAK inhibitors, baricitinib and tofacitinib. Three models were used to address whether JAKi affects bone: treatment (i) under steady-state conditions, (ii) in pathological bone loss during estrogen deficiency (OVX model), and (iii) in pathological bone loss during inflammation (arthritis model). In addition, patients with RA who received treatment with the JAK inhibitor tofacitinib were studied to detect signs of bone repair. To elucidate the mechanism of bone protection by JAKi, bone-forming osteoblasts and bone-degrading osteoclasts were analyzed regarding their function in the presence of JAK inhibitors. Investigation of all murine and human samples was performed in a blinded manner. The person scoring the mice and evaluating the histology, μCT, and immunological readout was unaware of the treatment mice had received. Mice were randomly assigned to experimental groups, which were distributed among cages to compensate for microbiome effects. At least three independent experimental runs were performed for all laboratory analysis in this study. Animal studies were approved by the ethics committees of the government of Unterfranken (Regierung von Unterfranken, Germany). Donors and patients gave written informed consent, and sample use for research was approved by the ethics committee of University Erlangen and complied with the World Medical Association Declaration of Helsinki–Ethical Principles for Medical Research Involving Human Subjects.

Murine ex vivo osteoclast differentiation assay

Bone marrow cells were isolated from the femur and tibia of 8- to 12-week-old C57BL/6 mice. After lysis of erythrocytes, cells were incubated overnight in osteoclast growth medium [α-minimum essential medium eagle (α-MEM) supplemented with 10% heat-inactivated fetal calf serum (FCS), penicillin (100 U/ml), and streptomycin (100 μg/ml) (all by Gibco)] to remove stromal cells by plastic adherence. The nonadherent cell fraction was seeded at 2×10^5 cells per well in a 96-well plate in growth medium supplemented with M-CSF (30 ng/ml; R&D Systems), RANKL (6 ng/ml; PeproTech), and incubated for 4 days with tofacitinib, baricitinib, or vehicle as indicated. To evaluate osteoclast differentiation, cells were stained for TRAP using a leukocyte acid phosphatase staining kit (Sigma-Aldrich) according to the manufacturer's manual. $TRAP^+$ cells with two or more nuclei were considered osteoclasts. For von Kossa stain, cells were plated in an osteo assay surface 96-well plate (Corning) and removed by osmotic lysis after 5 to 7 days. The remaining bone matrix was stained with 5% silver nitrate (Roth) for 30 min in the dark and developed with 5% sodium carbonate (Merck) in 25% formaldehyde (Roth) for 20 s. For the removal of unreacted silver, wells were washed with 5% sodium thiosulfate (Sigma-Aldrich) for 2 min. Pictures of the entire wells were captured. With image analysis software (Adobe Photoshop CS6 version 13.0.1), ratio of resorbed surface area in relation to whole surface area was quantified as a measurement of osteoclastic resorption capacity.

Human ex vivo osteoclast differentiation assay

All work with human cells was approved by the local ethics committee of University Erlangen and complies with the World Medical Association Declaration of Helsinki–Ethical Principles for Medical Research Involving Human Subjects. Human osteoclastogenesis assay was performed, according to Steffen *et al.* (*48*). Briefly, blood of normal healthy donors was collected in EDTA monovettes (Sarstedt) and diluted 1:1 with phosphate-buffered saline (PBS) (Gibco). Leukocyte fraction was isolated by density gradient centrifugation (Lymphoflot, Bio-Rad) and washed twice with chilled PBS supplemented with EDTA (1 mM; Roth). Cells were plated at a density of 3×10^6 cells per well in a 96-well plate in growth medium [α-MEM supplemented with penicillin (100 U/ml), streptomycin (100 μg/ml), and 10% heat-inactivated FCS (all Gibco)]. After 2 hours, medium was replaced with fresh growth medium, containing M-CSF (30 ng/ml), RANKL (3 ng/ml), and TGF-β (1 ng/ml) (all Peprotech). Medium was replaced every 3 days for a total duration of 6 to 8 days.

Osteogenic induction of MSCs

MSCs were isolated as previously described (*49*) from the bone marrow of C57BL/6 mice, following the MSC minimal criteria (*50*), and cultured in MSC growth medium [α-MEM supplemented with penicillin (100 U/ml), streptomycin (100 μg/ml) (all Gibco), and 10% heat-inactivated FCS (Biochrome)]. Cells were plated at 3×10^4 cells in 35-mm cell culture dishes. Upon reaching 100% confluency, medium was changed to either differentiation medium [MSC growth medium supplemented with L-ascorbic acid 2-phosphate sesquimagnesium salt hydrate (568 μM; Sigma-Aldrich)] or mineralization medium [(MSC growth medium supplemented with L-ascorbic acid 2-phosphate sesquimagnesium salt hydrate (568 μM; Sigma-Aldrich) and β-glycerol phosphate disodium salt pentahydrate (5 mM; Calbiochem)]. Medium contained vehicle, tofacitinib, or baricitinib as indicated and was changed three times a week. Alizarin Red staining was performed between days 4 and 6. To stain calcium deposits, cells were fixed with 95% ethanol and stained with 2% Alizarin Red (pH 4.2) (Sigma-Aldrich) for 2 min. Pictures of entire wells were captured. With image analysis software (Adobe Photoshop CS6 version 13.0.1), ratio of mineralized surface area in relation to whole surface area was quantified as a measurement of osteoblastic mineralization activity.

RNA isolation, complementary DNA synthesis, and qPCR

RNA isolation was performed according to the manufacturer's instructions using peqGOLD TriFast (VWR). Purity and concentration were assessed by spectrophotometry of 260 and 280 nm using the NanoDrop 1000 Spectrophotometer (Thermo Fisher Scientific) before first-strand complementary DNA (cDNA) synthesis, which was conducted with the MultiScribe Reverse Transcriptase system (Applied Biosystems), following the manufacturer's manual. qPCR performed in the QuantStudio 6 Flex Real-Time PCR System (Thermo Fisher Scientific), assessed the relative gene expression with SYBR Green I dNTP (deoxynucleotide triphosphate) (Eurogentec) according to the manufacturer's manual. For evaluation, relative expression (ΔCt), normalized to β-actin, and the ΔΔCt method were used. Primers used are listed in table S1.

μCT imaging and analysis

Tibiae were fixed in 4% paraformaldehyde overnight at 4°C and transferred to 70% ethanol. The proximal metaphyses of tibiae were scanned with cone-beam desktop μCT 40 (SCANCO Medical AG) with settings optimized for calcified tissue visualization (145 μA, 55 kVp, and 200-ms integration time for 500 projections per 180°). Segmentation of three-dimensional (3D) volumes was conducted

with the evaluation script Open VMS (Scanco Medical AG) containing adjusted grayscale thresholds and an isotropic voxel size of 8.4 μm. The analysis area started at 420 μm from the approximate middle of the growth plate and extending 1680 μm (200 tomograms) distally.

Enzyme-linked immunosorbent assay

Blood was harvested by cardiac puncture and serum separated with serum separation tubes (Becton Dickinson). Enzyme-linked immunosorbent assays (ELISAs; R&D Systems) were performed according to the instructions of the manufacturer's protocol. Serum concentrations of RANKL and OPG were measured undiluted and as 1:10 dilution in PBS, respectively.

Animal housing conditions

Mice were maintained in a specific pathogen–free facility with identical housing conditions controlling for the same environment and temperature at a 12-hour light/12-hour dark cycle, with free access to water and regular rodent chow. Experimental groups were distributed among cages to compensate for microbiome effects. The study was approved by the ethics committees of the Government of Unterfranken (Germany). Mice were obtained from Charles River Laboratories. Depending on the experiment, mice received tofacitinib (50 mg/kg), baricitinib (10 mg/kg) in 0.5% methylcellulose and 0.025% Tween solution, or vehicle only (0.5% methylcellulose and 0.025% Tween), as indicated, once or twice daily per oral gavage. The dosages of the two JAK inhibitors applied were based on previous works, with tofacitinib at 50 mg/kg twice daily, as exemplified by Ghoreschi *et al.* (*23*), and baricitinib dosing at 10 mg/kg twice daily by Fridman *et al.* (*26*). The divergence in tofacitinib and baricitinib administration was also reflected in varying dosing recommendations by both the European Medicines Agency and U.S. Food and Drug Administration, setting the dosage for tofacitinib at 5 to 10 mg/day and for baricitinib at 2 to 4 mg/day (*51*–*54*).

OVX-induced mouse model of osteoporosis

OVX was performed according to guidelines of laboratory animal care and use. For OVX, female C57BL/6 mice aged 8 weeks were anesthetized with a ketamine-xylazine solution and bilaterally ovariectomized, as previously described (*55*), whereas ovaries of sham mice were left intact. To ensure proper development of osteoporosis, mice were allowed to recover for 2 weeks, after which they started to receive tofacitinib (50 mg/kg), baricitinib (10 mg/kg), or vehicle twice daily for 6 weeks. Successful OVX was confirmed by assessment of uterus weight and weight development during the experiment.

K/BxN serum-transfer mouse model of arthritis

Serum from K/BxN mice, generated from breeding KRN TCR-transgenic mice with NOD/Lt mice, was collected and pooled. To induce arthritis, arthritogenic K/BxN serum (150 μl) was intraperitoneally injected into female C57BL/6 mice, aged 8 weeks. Simultaneously, mice started to receive tofacitinib (50 mg/kg), baricitinib (10 mg/kg), or vehicle twice daily per oral gavage for 2 weeks. A non–serum-induced healthy control group accompanied the experiment. Mice were scored for weight, grip strength, redness and swelling of hind paws (termed arthritis score) according to Chondrex, and footpad thickness and ankle thickness of hind paws monitored with dial thickness gauge (Peacock).

High-resolution quantitative computed tomography (HR-pQCT)

HR-pQCT scanning was performed with the high-resolution peripheral XtremeCT I scanner (Scanco Medical AG) with settings optimized for metacarpophalangeal joints (900 μA, 60 kVp, and 100-ms integration time for 750 projections per 180°). Segmentation of 3D volumes was conducted with the evaluation script Open VMS (Scanco Medical AG) containing adjusted grayscale thresholds and an isotropic voxel size of 82 μm, with 322 slices of analysis.

Whole transcriptome analysis (RNAseq)

RNAseq was performed at the next-generation sequencing core unit in the Institute of Human Genetics, University Hospital Erlangen, Friedrich-Alexander University Erlangen-Nuremberg. Samples were generated from at least 3 μg of high-quality RNA, with the Illumina TrueSeq Stranded mRNA Kit and sequenced on an Illumina HiSeq 2500 platform. Reads were purified from ribosomal RNA (rRNA), transfer RNA (tRNA), mitochondrial tRNAs (mt-tRNAs), and transposons by alignment against a custom reference list (BWA v0.7.14, SAMtools v1.8), and low-quality or masked bases, poly-A, and poly-T segments were removed (fqtrim v0.9.5). Quality of reads was determined on the raw data and after each processing step (fastqc v0.11.7). Reads were aligned against the *Mus musculus* reference genome (GRCm38, Ensembl 93) and quantified as the sum of nonoverlapping exonic reads per gene (SAMtools v1.8, subread v1.6.1). On the basis of this matrix, differentially expressed genes were determined (R v3.5.1, DESeq2 v1.20). Genes with a Benjamini-Hochberg–corrected FDR of $P < 0.1$ were considered for further cellular pathway analysis in ingenuity pathway analysis (QIAGEN Inc.; https://www.qiagen.com/se/products/discovery-and-translational-research/next-generation-sequencing/informatics-and-data/interpretation-content-databases/ingenuity-pathway-analysis) (*56*). RNAseq data are filed in the public database ArrayExpress with the accession number E-MTAB-8536.

Protein sampling, quantification, and Western blot analysis

For osteogenic induction, MSCs were plated at 3×10^4 cells per well in a six-well plate. At 100% confluency, medium was changed to differentiation medium. For sampling, cells were washed with ice-cold PBS (Gibco) and lysed in radioimmunoprecipitation assay buffer [PBS (Gibco) with 1% NP-40 (Roche), 0.5% sodium deoxycholate (Roth), and 0.1% SDS (Roth)] supplemented with 1× protease inhibitor cocktail, sodium orthovanadate (1 mM; both Sigma-Aldrich), and sodium fluoride (10 mM; VWR). After cell lysis, cellular debris was discarded by centrifugation. To adjust protein concentration, extracts were quantified with the DC Protein Assay Kit (Bio-Rad) according to the manufacturer's instructions and denatured in SDS sample buffer containing β-mercaptoethanol. Protein extracts were separated on 10, 12, and 15% SDS–polyacrylamide gels for anti-STAT/β-catenin, anti-Wnt, and anti-SOCS blotting, respectively, and transferred onto 0.2-μm nitrocellulose membranes (Bio-Rad). Membranes were blocked with 5% bovine serum albumin (Sigma-Aldrich) in tris-buffered saline solution with 0.05% Tween 20 (Roth) for 1 hour. Blots were probed with antibodies against phosphorylated targets and developed with Pierce ECL Western blotting substrate (Thermo Fisher Scientific) in a chemiluminescence imager (Biostep). For staining of unphosphorylated isoforms, blots were stripped with ReBlot Plus Strong Antibody Stripping Solution (Millipore) for 10 min, blocked, and probed as described earlier. Horseradish peroxidase–conjugated immunoglobulin

G (DAKO) was used as secondary antibody. Antibodies and controls used are depicted in table S2.

Histomorphometric analysis

For histological analyses, tibiae of mice were fixed in 4% paraformaldehyde overnight at 4°C and transferred to 70% ethanol. For toluidine blue (Fluka), hematoxylin and eosin (Merck, Sigma-Aldrich), and TRAP staining with a leukocyte acid phosphatase staining kit (Sigma-Aldrich), tibiae were decalcified in 14% EDTA (Sigma-Aldrich) adjusted to pH 7.2 with 25% ammonia hydroxide (Sigma-Aldrich) for 7 to 10 days until bone was pliable. Tibiae were then embedded in paraffin, and 2-µm sections were cut before respective staining. For Goldner trichrome staining, 5-µm methacrylate sections were prepared from undecalcified tibiae. Analysis was performed blinded using the OsteoMeasure histomorphometry system (OsteoMetrics Inc.) with a Zeiss Axioskop 2 microscope (Carl Zeiss AG).

Statistical analysis

Datasets are expressed as means ± SEM with sample sizes indicated in each legend. Outliers within datasets were excluded according to Grubb's test for variation from a normal distribution. Values below the detection limit were given values of zero. All statistical analyses were performed in Prism 5.03 (GraphPad) either by one-way repeated-measures analysis of variance (ANOVA) with Dunnett post hoc test, one-way ANOVA with Dunnett post hoc test, Wilcoxon signed-rank test, or two-tailed Mann-Whitney *U* test. Group differences were considered having a tendency toward significance or statistically significant when *P* value was less than 0.1 and 0.05, respectively. Raw data are reported in data file S1.

SUPPLEMENTARY MATERIALS

stm.sciencemag.org/cgi/content/full/12/530/eaay4447/DC1

Fig S1. JAKi does not affect cortical bone parameters or bone cell numbers under steady-state conditions.

Fig S2. Confirmation of OVX and cortical bone effects of JAKi after OVX.

Fig S3. Effects of JAKi on arthritis-mediated bone loss.

Fig S4. Gene network changes in MSCs during JAKi.

Fig. S5. Proposed model for the role of JAKi by baricitinib and tofacitinib in osteoblasts.

Table S1. Genetic targets and primers used for qPCR.

Table S2. Protein targets, antibodies, and control extracts used for Western blot analysis.

Data file S1. Raw data.

View/request a protocol for this paper from *Bio-protocol*.

REFERENCES AND NOTES

1. Y. Kobayashi, S. Uehara, N. Udagawa, N. Takahashi, Regulation of bone metabolism by Wnt signals. *J. Biochem.* **159**, 387–392 (2016).
2. R. Pacifici, The immune system and bone. *Arch. Biochem. Biophys.* **503**, 41–53 (2010).
3. H. Takayanagi, Osteoimmunology: Shared mechanisms and crosstalk between the immune and bone systems. *Nat. Rev. Immunol.* **7**, 292–304 (2007).
4. G. Mbalaviele, D. V. Novack, G. Schett, S. L. Teitelbaum, Inflammatory osteolysis: A conspiracy against bone. *J. Clin. Invest.* **127**, 2030–2039 (2017).
5. K. Hirahara, D. Schwartz, M. Gadina, Y. Kanno, J. J. O'Shea, Targeting cytokine signaling in autoimmunity: Back to the future and beyond. *Curr. Opin. Immunol.* **43**, 89–97 (2016).
6. S. Kim, T. Koga, M. Isobe, B. E. Kern, T. Yokochi, Y. E. Chin, G. Karsenty, T. Taniguchi, H. Takayanagi, Stat1 functions as a cytoplasmic attenuator of Runx2 in the transcriptional program of osteoblast differentiation. *Genes Dev.* **17**, 1979–1991 (2003).
7. K. Tajima, H. Takaishi, J. Takito, T. Tohmonda, M. Yoda, N. Ota, N. Kosaki, M. Matsumoto, H. Ikegami, T. Nakamura, T. Kimura, Y. Okada, K. Horiuchi, K. Chiba, Y. Toyama, Inhibition of STAT1 accelerates bone fracture healing. *J. Orthop. Res.* **28**, 937–941 (2010).
8. J. B. Levy, C. Schindler, R. Raz, D. E. Levy, R. Baron, M. C. Horowitz, Activation of the JAK-STAT signal transduction pathway by oncostatin-M cultured human and mouse osteoblastic cells. *Endocrinology* **137**, 1159–1165 (1996).
9. S. Kaneshiro, K. Ebina, K. Shi, C. Higuchi, M. Hirao, M. Okamoto, K. Koizumi, T. Morimoto, H. Yoshikawa, J. Hashimoto, IL-6 negatively regulates osteoblast differentiation through the SHP2/MEK2 and SHP2/Akt2 pathways in vitro. *J. Bone Miner. Metab.* **32**, 378–392 (2014).
10. D. C. Lacey, P. J. Simmons, S. E. Graves, J. A. Hamilton, Proinflammatory cytokines inhibit osteogenic differentiation from stem cells: Implications for bone repair during inflammation. *Osteoarthr. Cartil.* **17**, 735–742 (2009).
11. Drug Databases: OLUMIANT (2018). Drugs@FDA: FDA-Approved Drugs. [online] Available at: https://www.accessdata.fda.gov/scripts/cder/daf/index.cfm?event=overview.process&varApplNo=207924 [Accessed 31 Jan. 2020].
12. Drug Databases: XELJANZ (2012). Drugs@FDA: FDA-Approved Drugs. [online] Available at: https://www.accessdata.fda.gov/scripts/cder/daf/index.cfm?event=overview.process&ApplNo=203214 [Accessed 31 Jan. 2020].
13. Assessment report: Olumiant, international non-proprietary name: baricitinib. Procedure No. EMEA/H/C/004085/0000 (2016). European medicines agency [online] available at https://www.ema.europa.eu/en/documents/assessment-report/olumiant-epar-public-assessment-report_en.pdf [Accessed 31 Jan. 2020].
14. Assessment report: Xeljanz, international non-proprietary name: tofacitinib. Procedure No. EMEA/H/C/004214/0000 (2017). European medicines agency [online] available at https://www.ema.europa.eu/en/documents/assessment-report/xeljanz-epar-public-assessment-report_en.pdf [Accessed 31 Jan. 2020].
15. I. B. McInnes, G. Schett, The pathogenesis of rheumatoid arthritis. *N. Engl. J. Med.* **365**, 2205–2219 (2011).
16. J. D. Clark, M. E. Flanagan, J. B. Telliez, Discovery and development of Janus kinase (JAK) inhibitors for inflammatory diseases. *J. Med. Chem.* **57**, 5023–5038 (2014).
17. R. F. van Vollenhoven, Small molecular compounds in development for rheumatoid arthritis. *Curr. Opin. Rheumatol.* **25**, 391–397 (2013).
18. K. L. Winthrop, The emerging safety profile of JAK inhibitors in rheumatic disease. *Nat. Rev. Rheumatol.* **13**, 234–243 (2017).
19. D. van der Heijde, M. Dougados, Y. C. Chen, M. Greenwald, E. Drescher, R. Klar, L. Xie, I. de la Torre, T. P. Rooney, S. L. Witt, D. E. Schlichting, S. de Bono, P. Emery, Effects of baricitinib on radiographic progression of structural joint damage at 1 year in patients with rheumatoid arthritis and an inadequate response to conventional synthetic disease-modifying antirheumatic drugs. *RMD Open* **4**, e000662 (2018).
20. D. van der Heijde, Y. Tanaka, R. Fleischmann, E. Keystone, J. Kremer, C. Zerbini, M. H. Cardiel, S. Cohen, P. Nash, Y. W. Song, D. Tegzova, B. T. Wyman, D. Gruben, B. Benda, G. Wallenstein, S. Krishnaswami, S. H. Zwillich, J. D. Bradley, C. A. Connell, Tofacitinib (CP-690,550) in patients with rheumatoid arthritis receiving methotrexate: twelve-month data from a twenty-four-month phase III randomized radiographic study. *Arthritis Rheum.* **65**, 559–570 (2013).
21. T. P. LaBranche, M. I. Jesson, Z. A. Radi, C. E. Storer, J. A. Guzova, S. L. Bonar, J. M. Thompson, F. A. Happa, Z. S. Stewart, Y. Zhan, C. S. Bollinger, P. N. Bansal, J. W. Wellen, D. P. Wilkie, S. A. Bailey, P. T. Symanowicz, M. Hegen, R. D. Head, N. Kishore, G. Mbalaviele, D. M. Meyer, JAK inhibition with tofacitinib suppresses arthritic joint structural damage through decreased RANKL production. *Arthritis Rheum.* **64**, 3531–3542 (2012).
22. K. Murakami, Y. Kobayashi, S. Uehara, T. Suzuki, M. Koide, T. Yamashita, M. Nakamura, N. Takahashi, H. Kato, N. Udagawa, Y. Nakamura, A Jak1/2 inhibitor, baricitinib, inhibits osteoclastogenesis by suppressing RANKL expression in osteoblasts in vitro. *PLOS ONE* **12**, e0181126 (2017).
23. K. Ghoreschi, M. I. Jesson, X. Li, J. L. Lee, S. Ghosh, J. W. Alsup, J. D. Warner, M. Tanaka, S. M. Steward-Tharp, M. Gadina, C. J. Thomas, J. C. Minnerly, C. E. Storer, T. P. LaBranche, Z. A. Radi, M. E. Dowty, R. D. Head, D. M. Meyer, N. Kishore, J. J. O'Shea, Modulation of innate and adaptive immune responses by tofacitinib (CP-690,550). *J. Immunol.* **186**, 4234–4243 (2011).
24. K. Migita, A. Komori, T. Torigoshi, Y. Maeda, Y. Izumi, Y. Jiuchi, T. Miyashita, M. Nakamura, S. Motokawa, H. Ishibashi, CP690,550 inhibits oncostatin M-induced JAK/STAT signaling pathway in rheumatoid synoviocytes. *Arthritis Res. Ther.* **13**, R72 (2011).
25. S. P. Wang, S. Iwata, S. Nakayamada, K. Sakata, K. Yamaoka, Y. Tanaka, Tofacitinib, a JAK inhibitor, inhibits human B cell activation in vitro. *Ann. Rheum. Dis.* **73**, 2213–2215 (2014).
26. J. S. Fridman, P. A. Scherle, R. Collins, T. C. Burn, Y. Li, J. Li, M. B. Covington, B. Thomas, P. Collier, M. F. Favata, X. Wen, J. Shi, R. McGee, P. J. Haley, S. Shepard, J. D. Rodgers, S. Yeleswaram, G. Hollis, R. C. Newton, B. Metcalf, S. M. Friedman, K. Vaddi, Selective inhibition of JAK1 and JAK2 is efficacious in rodent models of arthritis: Preclinical characterization of INCB028050. *J. Immunol.* **184**, 5298–5307 (2010).
27. J. Choi, M. L. Cooper, K. Staser, K. Ashami, K. R. Vij, B. Wang, L. Marsala, J. Niswonger, J. Ritchey, B. Alahmari, S. Achilefu, I. Tsunoda, M. A. Schroeder, J. F. DiPersio, Baricitinib-induced blockade of interferon gamma receptor and interleukin-6 receptor for the prevention and treatment of graft-versus-host disease. *Leukemia* **32**, 2483–2494 (2018).
28. C. Pilling, J. A. Cooper, SOCS2 binds to and regulates EphA2 through multiple mechanisms. *Sci. Rep.* **7**, 10838 (2017).
29. J. L. Tong, L. L. Wang, X. F. Ling, M. X. Wang, W. Cao, Y. Y. Liu, MiR-875 can regulate the proliferation and apoptosis of non-small cell lung cancer cells via targeting SOCS2. *Eur. Rev. Med. Pharmacol. Sci.* **23**, 5235–5241 (2019).

30. J. Li, JAK-STAT and bone metabolism. *JAKSTAT* **2**, e23930 (2014).
31. S. Itoh, N. Udagawa, N. Takahashi, F. Yoshitake, H. Narita, S. Ebisu, K. Ishihara, A critical role for interleukin-6 family-mediated Stat3 activation in osteoblast differentiation and bone formation. *Bone* **39**, 505–512 (2006).
32. N. A. Sims, B. J. Jenkins, J. M. Quinn, A. Nakamura, M. Glatt, M. T. Gillespie, M. Ernst, T. J. Martin, Glycoprotein 130 regulates bone turnover and bone size by distinct downstream signaling pathways. *J. Clin. Invest.* **113**, 379–389 (2004).
33. B. Peruzzi, A. Cappariello, A. Del Fattore, N. Rucci, F. De Benedetti, A. Teti, c-Src and IL-6 inhibit osteoblast differentiation and integrate IGFBP5 signalling. *Nat. Commun.* **3**, 630 (2012).
34. R. Pacifici, Role of T cells in ovariectomy induced bone loss–revisited. *J. Bone Miner. Res.* **27**, 231–239 (2012).
35. M. Ito, S. Yamazaki, K. Yamagami, M. Kuno, Y. Morita, K. Okuma, K. Nakamura, N. Chida, M. Inami, T. Inoue, S. Shirakami, Y. Higashi, A novel JAK inhibitor, peficitinib, demonstrates potent efficacy in a rat adjuvant-induced arthritis model. *J. Pharmacol. Sci.* **133**, 25–33 (2017).
36. M. M. Matzelle, M. A. Gallant, K. W. Condon, N. C. Walsh, C. A. Manning, G. S. Stein, J. B. Lian, D. B. Burr, E. M. Gravallese, Resolution of inflammation induces osteoblast function and regulates the Wnt signaling pathway. *Arthritis Rheum.* **64**, 1540–1550 (2012).
37. D. Diarra, M. Stolina, K. Polzer, J. Zwerina, M. S. Ominsky, D. Dwyer, A. Korb, J. Smolen, M. Hoffmann, C. Scheinecker, D. van der Heide, R. Landewe, D. Lacey, W. G. Richards, G. Schett, Dickkopf-1 is a master regulator of joint remodeling. *Nat. Med.* **13**, 156–163 (2007).
38. R. Baron, M. Kneissel, WNT signaling in bone homeostasis and disease: From human mutations to treatments. *Nat. Med.* **19**, 179–192 (2013).
39. V. Krishnan, H. U. Bryant, O. A. Macdougald, Regulation of bone mass by Wnt signaling. *J. Clin. Invest.* **116**, 1202–1209 (2006).
40. S. Ye, D. Zhang, F. Cheng, D. Wilson, J. Mackay, K. He, Q. Ban, F. Lv, S. Huang, D. Liu, Q. L. Ying, Wnt/β-catenin and LIF-Stat3 signaling pathways converge on Sp5 to promote mouse embryonic stem cell self-renewal. *J. Cell Sci.* **129**, 269–276 (2016).
41. M. A. Fragoso, A. K. Patel, R. E. Nakamura, H. Yi, K. Surapaneni, A. S. Hackam, The Wnt/β-Catenin pathway cross-talks with STAT3 signaling to regulate survival of retinal pigment epithelium cells. *PLOS ONE* **7**, e46892 (2012).
42. K. Matsushita, S. Itoh, S. Ikeda, Y. Yamamoto, Y. Yamauchi, M. Hayashi, LIF/STAT3/SOCS3 signaling pathway in murine bone marrow stromal cells suppresses osteoblast differentiation. *J. Cell. Biochem.* **115**, 1262–1268 (2014).
43. M. T. Cantwell, J. S. Farrar, J. C. Lownik, J. A. Meier, M. Hyun, V. Raje, M. R. Waters, F. S. Celi, D. H. Conrad, T. E. Harris, A. C. Larner, STAT3 suppresses Wnt/β-catenin signaling during the induction phase of primary Myf5+ brown adipogenesis. *Cytokine* **111**, 434–444 (2018).
44. M. Shin, E. H. Yi, B. H. Kim, J. C. Shin, J. Y. Park, C. H. Cho, J. W. Park, K. Y. Choi, S. K. Ye, STAT3 potentiates SIAH-1 mediated proteasomal degradation of β-catenin in human embryonic kidney cells. *Mol. Cells* **39**, 821–826 (2016).
45. J. Chang, W. Sonoyama, Z. Wang, Q. Jin, C. Zhang, P. H. Krebsbach, W. Giannobile, S. Shi, C. Y. Wang, Noncanonical Wnt-4 signaling enhances bone regeneration of mesenchymal stem cells in craniofacial defects through activation of p38 MAPK. *J. Biol. Chem.* **282**, 30938–30948 (2007).
46. C. A. O'Brien, I. Gubrij, S. C. Lin, R. L. Saylors, S. C. Manolagas, STAT3 activation in stromal/osteoblastic cells is required for induction of the receptor activator of NF-kappaB ligand and stimulation of osteoclastogenesis by gp130-utilizing cytokines or interleukin-1 but not 1,25-dihydroxyvitamin D3 or parathyroid hormone. *J. Biol. Chem.* **274**, 19301–19308 (1999).
47. P. Garnero, E. Thompson, T. Woodworth, J. S. Smolen, Rapid and sustained improvement in bone and cartilage turnover markers with the anti-interleukin-6 receptor inhibitor tocilizumab plus methotrexate in rheumatoid arthritis patients with an inadequate response to methotrexate: results from a substudy of the multicenter double-blind, placebo-controlled trial of tocilizumab in inadequate responders to methotrexate alone. *Arthritis Rheum.* **62**, 33–43 (2010).
48. U. Steffen, F. T. Andes, G. Schett, Generation and analysis of human and murine osteoclasts. *Curr. Protoc. Immunol.* **125**, e74 (2019).
49. C. Bouffi, C. Bony, G. Courties, C. Jorgensen, D. Noel, IL-6-dependent PGE2 secretion by mesenchymal stem cells inhibits local inflammation in experimental arthritis. *PLOS ONE* **5**, e14247 (2010).
50. M. Dominici, K. Le Blanc, I. Mueller, I. Slaper-Cortenbach, F. Marini, D. Krause, R. Deans, A. Keating, D. Prockop, E. Horwitz, Minimal criteria for defining multipotent mesenchymal stromal cells. The international society for cellular therapy position statement. *Cytotherapy* **8**, 315–317 (2006).
51. Oluminat (European Medicine Agency, 2016), vol. 2019, pp. procedure no. EMEA/H/C/004085/000000/.
52. Xeljanz (European Medicine Agency, 2017), vol. 2019, pp. procedure no. EMEA/H/C/004214/0000.
53. Medication guide, full prescribing information: Xeljanz (4269956) (FDA, 2018).
54. Medication guide, full prescribing information: Olumiant (4271150) (FDA, 2018).
55. A. I. Idris, Ovariectomy/orchidectomy in rodents. *Methods Mol. Biol.* **816**, 545–551 (2012).
56. A. Krämer, J. Green, J. Pollard Jr., S. Tugendreich, Causal analysis approaches in ingenuity pathway analysis. *Bioinformatics* **30**, 523–530 (2014).

Acknowledgments: We thank F. Djouad for providing the MSCs; B. Happich and H. Symowski for technical assistance; A. B. Ekici, P. Kirchner, M. Herrmann, and M. Hoffmann for discussion of the data; and L. Schuster, M. Stock, J. Behrens, M. Brückner, and W. Baum for scientific support. **Funding:** This work was supported by the Deutsche Forschungsgemeinschaft (FOR 2886 PANDORA project no. TP3/TP4/TP5), DFG-CRC 1181 project no. A01/A03/A05, project SCHE (1583/14-1), project HA 8163/1-1, research grants from Eli Lilly and Pfizer, the Bundesministerium für Bildung und Forschung (BMBF) (METARTHROS), the European Union (ERC StG 640087–SOS and ERC 4D NanoScope) and the EU/EFPIA Innovative Medicines Initiative 2 Joint Undertaking RTCure grant no. 777357, and the Interdisciplinary Center for Clinical Research (IZKF) at the Universitätsklinikum Erlangen of the Friedrich-Alexander-University Erlangen-Nürnberg. **Author contributions:** Conceptualization: A.K., G.K., and A.J.H. Methodology: S.A. Validation: S.A., N.S., and U.S. Formal analysis: S.A., N.S., U.S., and D.W. Investigation: S.A., N.S., U.S., F.T.A., D.W., A.K., S.C., and M.H. Resources: U.S., F.T.A., C.S., D.I.H.M., and D.A. Data curation: S.A. Writing (original draft): S.A. and G.S. Writing (review and editing): S.A., G.S., G.K., S.F., and A.J.H. Visualization: S.A. Supervision: C.S., G.S., G.K., S.F., and A.J.H. Project administration: S.A., G.K., S.F., and A.J.H. Funding acquisition: G.K. and A.J.H. **Competing interests:** A.K. received consulting fees from Eli Lilly. A.J.H. received consulting fees from AbbVie, BMS, GSK, Janssen, Roche, Eli Lilly, and Novartis. The other authors declare that they have no competing interests. **Data and materials availability:** All data associated with this study are present in the paper or the Supplementary Materials. The RNAseq datasets have been deposited in the public database ArrayExpress with accession number E-MTAB-8536.

Submitted 28 June 2019
Accepted 8 January 2020
Published 12 February 2020
10.1126/scitranslmed.aay4447

Citation: S. Adam, N. Simon, U. Steffen, F. T. Andes, C. Scholtysek, D. I. H. Müller, D. Weidner, D. Andreev, A. Kleyer, S. Culemann, M. Hahn, G. Schett, G. Krönke, S. Frey, A. J. Hueber, JAK inhibition increases bone mass in steady-state conditions and ameliorates pathological bone loss by stimulating osteoblast function. *Sci. Transl. Med.* **12**, eaay4447 (2020).

Science Translational Medicine

JAK inhibition increases bone mass in steady-state conditions and ameliorates pathological bone loss by stimulating osteoblast function

Susanne Adam, Nils Simon, Ulrike Steffen, Fabian T. Andes, Carina Scholtysek, Dorothea I. H. Müller, Daniela Weidner, Darja Andreev, Arnd Kleyer, Stephan Culemann, Madelaine Hahn, Georg Schett, Gerhard Krönke, Silke Frey and Axel J. Hueber

Sci Transl Med **12**, eaay4447.
DOI: 10.1126/scitranslmed.aay4447

Boosting osteoblasts to battle bone erosion

Inhibitors of Janus kinase (JAK) reduce inflammation and are approved to treat rheumatoid arthritis; however, the direct effects of inhibitors on bone remain unclear. Adam *et al.* found that JAK inhibitors increased bone mass in mice under homeostatic conditions and mitigated bone loss in a mouse model of osteoporosis. Mice with inflammatory bone loss mimicking rheumatoid arthritis had reduced bone erosions after treatment with JAK inhibitors, and two patients with rheumatoid arthritis treated with tofacitinib showed similar results. The authors determined that JAK inhibitors induced bone repair by altering gene expression and increasing activity of osteoblasts, supporting use of inhibitors as potential osteoanabolics.

Science Translational Medicine (ISSN 1946-6242) is published by the American Association for the Advancement of Science, 1200 New York Avenue NW, Washington, DC 20005. The title *Science Translational Medicine* is a registered trademark of AAAS.